Development of Humanoid Robot Head Based on FACS

Nguyen Khac Toan, Le Duc Thuan, Le Bao Long, and Nguyen Truong Thinh
Department of Mechatronics, Ho Chi Minh City University of Technology and Education, Thu Duc City, Ho Chi Minh City, Vietnam
Email: khactoan240@gmail.com, leducthuan0987@gmail.com, lebaolong169@gmail.com, thinhnt@hcmute.edu.vn

***Abstract*—Advances in artificial intelligence have allowed humanoid robots to communicate and serve human needs. However, displays are often used for humanoid robots to perform expressions, limiting the authenticity and naturalness of human-robot interactions. This paper presents the design and analysis method of the humanoid robot head to improve interoperability. At first, the Facial Action Coding System (FACS) was used to determine which Action units were required to perform expressions. Control points are required to generate Action units, and they are determined based on the action of facial muscles. In the next step, the humanoid robot head is divided into 3 parts: eyes, jaw-lip, and neck. Each section was dug into anatomy to research the shape, size, and range of motion of bones and joints. Mechanisms are designed based on this data to realistically simulate the structure and motion of individual parts of the human head. In addition, the forward and inverse kinematics problems of each mechanism are also solved to determine the control equation of each control point and workspace. These results demonstrated the theoretical operability of mechanisms that are suitable for simulating human facial motions. Finally, a humanoid robot head is implemented based on this method to evaluate the capability to simulate motion and perform expression. Experiment results show the simulation rate is up to 94.72%, and the expression recognition rate is 89.93%.**

***Index Terms*—humanoid robotic head, mechanisms, FACS, Facial Action Coding System, robotic emotion**

I. Introduction

Robot is a term which is no longer strange to humans. The constant development of science has given rise to the birth of more advanced robots. Various types of robots were developed in different shapes such as animal robots [1], interaction robot [2]. The robots all share the same goal of assisting and interacting with humans. The researchers are focusing on creating robots with friendly appearances and capable of generating precise facial expressions. Therefore, humanoid robot was developed, this is a different type of anthropomorphic robot which can imitate or reproduce human movements. This type of robot is drawing a lot of attention and is at the center of many different research projects around the world. Psychologists' studies show that only 7% of information is transferred by spoken language, while 38% is expressed by paralanguage and 55% is transferred by facial expressions. It can be seen that, facial expression robot continues to enter the people's lives, which will be an inevitable trend [3].

In the past few years, there has been a great increase in the number of robot head projects, which set a huge positive impact on the robotics field. Romeo robot can rotate the eye up to 400°/s [4]. Ciprian author team created a robot head which can perform neck rotation up to 55° [5]. Flobi robot was capable of displaying five basic facial expressions [6]. However, in the past few years, robot makers have no longer focused too much on creating a human-like appearance for robots, but only focused on developing artificial intelligence. Most robots built since 2016 have an interactive screen on the head and express emotions through images on the screen. There are various examples such as teaching assistant robot RASA [7], ENRICHME robot serves as assistant for the elderly [8]. This has made the appearance of the robots become less friendly and made the process of conveying the emotions of the robot to humans more difficult. Therefore, modifying the mechanisms in order to make the expressions more realistic is necessary.

This paper is aimed to make a humanoid robot head which is shaped and sized like a human head and can generating highly realistic expressions. The paper is organized as follows: in Section 2 we introduce about the method to create facial expressions by using Facial Action Coding System (FACS). Section 3 explains the kinematics analysis of mechanisms which built the robot head. In Section 4 we test the robot head through experiments. Section 5 presents conclusion and future work for the robot head.

II. Methodology

Facial Action Coding System (FACS) was developed by Ekman and Friesen in 1978 to objectively measure facial activity for behavioral science investigations of the face, which provided an objective description of facial signals in terms of component motions, or "facial actions" [9]. FACS defined movement of the face through "Action Units" or AUs [10]. There are 46 action units and each of them is formed by several muscles on the face. Difference changes in facial expression are encoded by FACS into specific facial muscle movements [11].

Manuscript received November 16, 2021; revised February 2, 2022.

doi: 10.18178/ijmerr.11.5.365-372

Various AUs can be freely combined together to create different facial expressions. It is a widely used standard for categorizing the appearance of facial expressions.

One of the most critical components in developing facial expressions is selecting correct position of control points and direction of skin motion on the robot head [12]. By applying anatomical knowledge in [13], we were able to define 26 control points on the face of the robot as shown in Fig. 1. Each point was driven by a different mechanism, from the combination of a certain number of points, 24 AUs can be created as shown in Table I. These 24 AUs are the components of 6 basic facial expressions shown in Table II: happy, sad, angry, surprise, disgust and fear. The movement of mechanisms that control the points will be explained in detail in Section 3 below.

TABLE I. CONTROL POINTS MAKE UP THE AUS

AU	Control point		Appearance changes
	Right	***Left***	
1	3	2	Inner Brow Raiser
2	4	1	Outer Brow Raiser
4	4, 3	1, 2	Brow Lowerer
5	6	5	Upper Lid Raiser
6	12	11	Cheek Raiser
7	6, 10	5, 9	Lid Tightener
9	14	13	Nose Wrinkler
10	25	23	Upper Lip Raiser
12	20, 12	19, 11	Lip Corner Puller
14	20	19	Dimpler
15	20	19	Lip Corner Depressor
16	26, 24, 22		Lower Lip Depressor
18	19, 21, 23, 25, 20, 26, 24, 22		Lip Puckerer
25	19, 20, 26, 24, 22		Lips Part
26	15	16	Jaw Drop
27	15	16	Mouth Stretch
29	17	18	Jaw Thrust
43	6	5	Eyes Closed
45	6, 10	5, 9	Blink
46	6, 10	5, 9	Wink
61	8	7	Eyes Turn Left
62	8	7	Eyes Turn Right
63	8	7	Eyes Up
64	8	7	Eyes Down

TABLE II. AUS MAKE UP THE SIX BASIC FACIAL EXPRESSION

Expressions	AUs
Surprise	1 + 2 + 5 + 7 + 20 + 16
Happy	6 + 7 + 12
Disgust	9 + 10 + 15 + 16
Sad	1 + 4 + 15
Anger	4 + 5 + 7 + 9
Fear	1 + 2 + 5 + 26

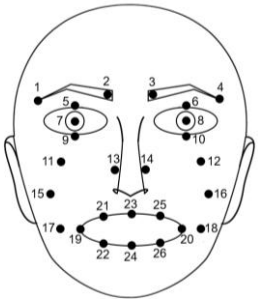

Figure 1. Control points in the face.

III. MECHANISM DESIGN

A. Eye Mechanism

The largest structure of the eye is approximately spherical with a radius of around 11.5mm [14]. There is variation in size between individuals but the average axial length of the globe is 24mm (range 21 – 26). The Inter-Pupillary Distance (IPD) (which is the distance between the centers of the two pupils) has an average range of 56 to 72 mm. The eye performs approximately a range of motion of 35 ° up and down, to the right and to the left [15]. The parameters of the eyelids are measured to be 30 ° from horizontal for both lids in the wide state, 26.8 ° from horizontal for both lids for the neutral state, and the bottom eyelid is 22 ° from the horizontal [16]. By applying the anatomical knowledge of the eye [17], it can be deduced that the eye is controlled by 6 muscles. Roll, pitch and yaw are 3 degrees of freedom (DOF) of the eye. However, it can easily be seen that there is not any human expression related to the roll motion. Therefore, the roll motion will be removed. The eyeballs will have two degrees of freedom, while the eyelids will have one.

Fig. 2 shown the design of the eye-pitch mechanism and eyelids mechanism, which is a 4-bar planar linkage. The initial state of the eye mechanism is described by points connected by links in black color, the points connected by links in light color describe the final state. Point A is the location of eyeball center, point D is the location of the motor, the pupil is put at point E. In order to simplify the control process, eye-pitch mechanism was designed in a parallelogram. α addresses for the revolution angle of AB around A, β addresses for the revolution angle of CD around D. γ addresses for the revolution angle of EA around A. Using velocity analysis, it can easily be seen that

$$\alpha = \beta = \gamma . \tag{1}$$

Fig. 3 describes the eye-yaw mechanism, which is also a 4-bar planar linkage. The motor is placed at point C, 2 centers of the eyeballs is put at points A and E. Points G and H represent for the pupils. The initial and final state of the mechanism are described the same as Fig. 2. In order to simplify the calculations, ABFE will be designed in a parallelogram. α addresses for the revolution angle of AB around A, β addresses for the revolution angle of CD around C. γ addresses for the revolution angle of EF

around E. The relationship between α, γ and β can easily be determined as

$$\alpha = \beta = \gamma . \tag{2}$$

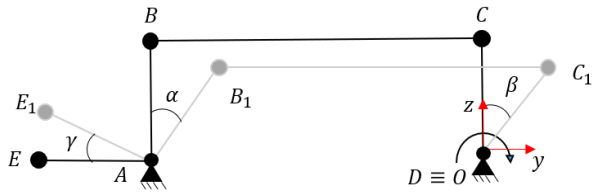

Figure 2. Kinematic diagram of eye-pitch mehanism.

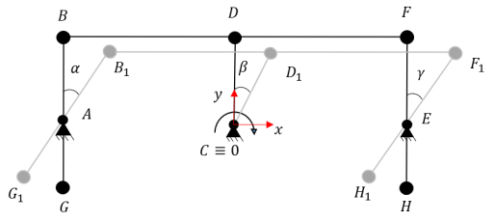

Figure 3. Kinematic diagram of eye-yaw mehanism.

B. Lip Mechanism

The lips, which surround the oral cavity, are vital for creating facial expressions. An important component of the speech apparatus, the lips are involved in the creating of bilabial (m, p, b) and labiodental (f, v) consonant sounds and vowel rounding/labialization [18]. On the anterior view, the upper red lip height should be less than the lower red lip height, and the upper lip should project approximately 2 mm more than the lower lip on profile [19]. There are 11 muscles controlling the lip movement. One of them is the Orbicularis oris, which acts as a sphincter around the mouth. This muscle is crucial for creating shape for the mouth when talking.

As shown in Fig. 1, there are 8 control points related to the lips includes: 19, 20, …, 26. It is necessary to choose suitable mechanism for controlling the movements of these points. The 4-bar planar mechanism is our selection. However, we have modified it in to the parallelogram form shown in Fig. 4, this makes the kinematics analyzing become easier. Point 19 and 20 are 2 points that have a quite complex moving trajectory, they are driven by 5-bars planar mechanisms, which leads to much more complicated calculations. The following section mainly performs the inverse and forward kinematics analysis of the 5-bar planar mechanism.

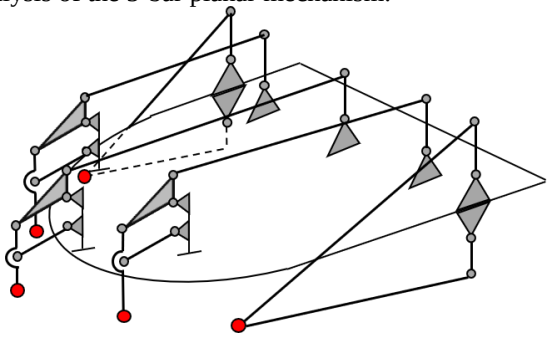

Figure 4. Top-lip mechanism.

1) Forward Kinematics

Points 19 and 20 are both driven by 5-bar planar mechanism, the kinematic diagram and workspace of the mechanism are shown in Fig. 5. δ addresses for the revolution angle of the motor at M, ε addresses for the revolution angle of the motor at R. The position of point N' and point Q' in the coordinate system Ox'y'z' are determined as follows:

$$\begin{aligned} N' &= (0, MN\cos\delta, -MN\sin\delta) \\ Q' &= (0, -RQ\cos\varepsilon, RQ\sin\varepsilon) \end{aligned} \tag{3}$$

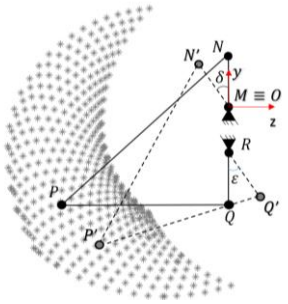

Figure 5. Workspace and kinematic diagram of lip corner mechanism.

The equations below describe the coordinates of point P':

$$\begin{cases} (y_{P'} - y_{N'})^2 + (z_{P'} - z_{N'})^2 = NP^2 \\ (y_{P'} - y_{Q'})^2 + (z_{P'} - z_{Q'})^2 = PQ^2 \end{cases} \tag{4}$$

Solve equation (4):

$$z_P = \frac{(y_N - z_Q)(-A^2 - 4.A.NP.PQ)^{(1/2)} + B + C}{-2(NM^2 + MR(2y_N + MR) + D)} \tag{5}$$

$$\begin{aligned} y_P = {} & \frac{y_N^2 - (MR + QR\cos(\varepsilon))^2 - NP^2 + PQ^2}{2MR + 2y_N + 2QR\cos(\varepsilon)} \\ & + \frac{(z_P - z_N)^2 - (z_P - z_Q)^2}{2MR + 2y_N + 2QR\cos(\varepsilon)} \end{aligned} \tag{6}$$

Where:

$$\begin{aligned} A &= MN^2 + 2MRy_N + 2MN.QR\cos(\delta - \varepsilon) + MR^2 \\ &\quad + 2MR.QR\cos(\varepsilon) - NP^2 - 2NP.PQ - PQ^2 + QR^2 \\ B &= MN^2(-z_N + MR\sin(2\delta) - \cos(2\delta)z_Q \\ &\quad + QR\cos(\varepsilon)\sin(2\delta)) + QR^2(-z_Q - MR\sin(2\varepsilon) \\ &\quad - \cos(2\varepsilon)z_N - y_N\sin(2\varepsilon)) + MR^2.MN\sin(\varepsilon) \\ &\quad - 2MR.QR\cos(\varepsilon)z_N \\ C &= (\mathrm{NP}^2 - PQ^2)(z_N - z_Q) - MR^2 z_Q - 2MR.y_N.z_Q \\ D &= PQ(2MN\cos(\delta - \varepsilon) + 2MR\cos(\varepsilon) + QR) \end{aligned} \tag{7}$$

2) Inverse Kinematics

Given the coordinates of point P'=($x_{P'}$,$y_{P'}$), δ and ε are rotation angles of the motors placed at M and R. Equation (4) can be rewritten as:

$$(y_{P'} - MN\cos\delta)^2 + (z_{P'} + MN\sin\delta)^2 = NP^2 \tag{8}$$

Applying $\cos\delta = \frac{1-u^2}{1+u^2}$ on equation (8):

$$\frac{Eu^2+F}{u^2+1} = 0 \tag{9}$$

Where:

$$\begin{aligned} E &= MN^2 + 2MNy_{P'} + 4MNz_{P'} - NP^2 + y_{P'}^2 + z_{P'}^2 \\ F &= MN^2 - 2MNy_{P'} - NP^2 + y_{P'}^2 + z_{P'}^2 \end{aligned} \tag{10}$$

Equation (9) can be rewritten as:

$$\delta = 2\arctan\left(\sqrt{\frac{-F}{E}}\right) \tag{11}$$

The equation of angle ε is:

$$\left(y_{P'} + QR\cos\varepsilon\right)^2 + \left(z_{P'} - QR\sin\varepsilon\right)^2 = PQ^2 \tag{12}$$

$$\Rightarrow \varepsilon = 2\arctan\left(\sqrt{\frac{-K}{J}}\right) \tag{13}$$

Where:

$$\begin{aligned} J &= QR^2 + 2QRy_{P'} + 4QRz_{P'} - PQ^2 + y_{P'}^2 + z_{P'}^2 \\ K &= QR^2 - 2QRy_{P'} - PQ^2 + y_{P'}^2 + z_{P'}^2 \end{aligned} \tag{14}$$

C. Jaw Mechansim

In the adult, the skull consists of 22 individual bones, 21 of which are immobile and united into a single unit. The 22nd bone is the mandible (lower jaw), which is the only moveable bone of the skull [20]. The mandible is the largest of the facial bones. It is a very mobile bone, suspended from the cranium by muscles, ligaments, and the capsule of TMJ (temporomandibular joint). Muscle of massification attaches either directly or indirectly to the mandible [13]. It supports the lower teeth and provides attachment for muscles of mastication and facial expression [17]. The angular measurements of the rotation of the mandibular ramus were 39.1±5.9° in men and 36.3±4.3° in women [21].

FACS defines 46 AUs, only 5 AUs relate to the movement of the jaw includes: Jaw Drop, Mouth Stretch, Jaw Thrust, Jaw Sideways, Jaw Clencher. There hardly any facial expression related to the side movement of the mandible, therefore, Jaw Sideways will be omitted, 3 AUs remain are Jaw Drop, Mouth Stretch and Jaw Thrust. Movements of the mouth when talking or expressing emotions are mainly produced by the jaw mechanism. The following section focuses mainly on analyzing the forward and reverse kinematics of the mechanism, which will be the foundation for controlling the motor.

1) Forward kinematics

The jaw mechanism is shown in Fig. 6 in form of a 5-bar linkage. 4 points S, N, P and Q describes the initial state of the mechanism. The final state of the mechanism is described by 4 points S', N', P' and Q'. δ is the angle between MN and MN', the angle between RQ and RQ' is ε.

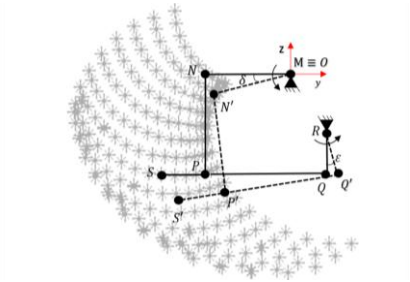

Figure 6. Workspace and kinematic diagram of jaw mechanism.

The coordinates of points N' and Q' can be deduced from the equations below:

$$\begin{aligned} N' &= \left(0, -MN\cos\delta, -MN\sin\delta\right) \\ Q' &= \left(0, QR\cos\varepsilon + y_R, -QR\sin\varepsilon + z_R\right) \end{aligned} \tag{15}$$

The coordinates of point P' are given as P'=($x_{P'}$,$y_{P'}$), the following equations determine the lengths of NP and PQ:

$$\begin{cases} (y_{P'} - y_{N'})^2 + (z_{P'} - z_{N'})^2 = NP^2 \\ (y_{P'} - y_{Q'})^2 + (z_{P'} - z_{Q'})^2 = PQ^2 \end{cases} \tag{16}$$

Solve the equations (16):

$$z_P = \frac{A + (y_Q - y_N)(-B^2 - 4B.\mathrm{NP}.\mathrm{PQ})^{(1/2)} + D}{2(\mathrm{MN}^2 + 2z_N MR + MR^2 + C)} \tag{17}$$

$$y_P = \frac{y_N^2 - y_Q^2 - NP^2 + PQ^2 + (z_P - z_N)^2 - (z_P - z_Q)^2}{2y_N - 2y_Q} \tag{18}$$

Where:

$$\begin{aligned} B &= MN^2 + 2MRz_B + 2MN.\mathrm{QR}\cos(\delta - \varepsilon) \\ &\quad + MR^2 + 2MR.\mathrm{QR}\cos(\varepsilon) - NP^2 \\ &\quad - 2NP.\mathrm{PQ} - PQ^2 + QR^2 \\ A &= -(\mathrm{MR}^2(\mathrm{MR} - 3z_Q\,\mathrm{QR}\cos(\varepsilon) \\ &\quad + MRz_N + y_N^2) + QR^3\cos(\varepsilon) \\ &\quad - NM^2 z_N + (\mathrm{PQ}^2 - NP^2)(z_Q - z_N) \\ D &= -z_N^2 MR + y_Q^2 MR + MN^2\,\mathrm{QR}\cos(2\delta - \varepsilon) \\ &\quad + QR^2\,\mathrm{MN}\sin(2\varepsilon - \delta) \\ &\quad - 2MN.\mathrm{MR}.\mathrm{QR}\sin(\delta - \varepsilon)) \\ C &= QR(2MR\cos\varepsilon - 2MN\sin(\delta - \varepsilon)) \end{aligned} \tag{19}$$

Three points S', P', Q' are collinear, and p = SQ/PQ, the equation of point S is shown below:

$$\overrightarrow{OS} = p.\overrightarrow{QP} + \overrightarrow{OQ} \tag{20}$$

2) Inverse kinematics

The equation (20) can be written as:

$$\begin{cases} y_{P'} = ky_{Q'} + (1-p)y_{S'} \\ z_{P'} = kz_{Q'} + (1-p)z_{S'} \end{cases} \tag{21}$$

By applying the same principle of lip mechanism, it can be deduced that:

$$\delta = 2\arctan\left(\sqrt{\frac{-E}{F}}\right); \varepsilon = 2\arctan\left(\sqrt{\frac{-G}{H}}\right) \quad (22)$$

Where:

$$\begin{aligned} E &= QR^2 - 2QRy_{S'} - SQ^2 + y_{S'}^2 + z_{S'}^2, \\ F &= QR^2 + 2QRy_{S'} + 4QRz_{S'} - SQ^2 + y_{S'}^2 + z_{S'}^2, \\ G &= MN^2 - 2MNy_{S'} - NP^2 + y_{S'}^2 + z_{S'}^2, \\ H &= MN^2 + 2MNy_{S'} + 4MNz_{S'} - NP^2 + y_{S'}^2 + z_{S'}^2, \end{aligned} \quad (23)$$

D. Neck Mechansim

The equilibrium of the head is control mainly by the neck. There are 7 cervical vertebrae (C1 – C7). Their function is to support the head and allow for its movements. The actions of the neck include flexion (tipping the head forward), extension (holding the head erect), hyperextension (as in looking upward), lateral flexion (tilting the head to one side), and rotation (turning the head to look left or right) [17]. The flexion movement of the neck with a canonical range of 50 degrees while the extension with a range of 57.5 degrees. The neck can turn the head to the right and to the left with a range of 70 degrees [15].

Mechanisms that replicate the movement of the human neck are classified as serial and parallel. Based on the function and action of the cervical vertebrae, the series mechanism is considered to be the suitable one for the neck due to its ease of control. With a large number of joints, this type of mechanism can achieve high flexibility. However, this is also why it has a high cumulative error and poor bearing capacity. Comparing serial robots with many other kinds of machines, they are characterized by low stiffness [22]. Parallel manipulators, on the contrary, possess many advantages such as high rigidity, large load capacity, great accuracy and high speed. Although this type of mechanism is difficult to control, the parallel mechanism will be used to simulate human neck motion due to its numerous advantages.

Fig. 7 depicts the mechanisms for simulating neck movements. In parallel mechanism, RSSR (R and S stand for revolute and spherical kinematic pairs respectively) it is the one with the most simulation potential. The neck mechanism consists of two main parts including the moving platform and the base platform. Points A, B and C are fixed point located at the base of the humanoid robot head. Two motors are placed at point B and C, BG and CH is the length of the motor's arms. Point D is located at the universal joint, points E, F, G and H are spherical joints.

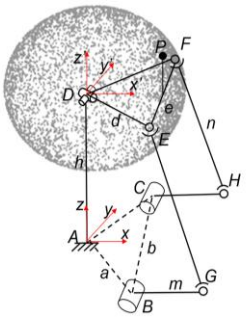

Figure 7. Workspace and kinematic diagram of neck mechanism.

Fig. 7 shows AB = AC = a, BC = b, BG = CH = m, EG = FH = n, DE = DF = d, EF = e, AD = h. Axyz is chosen as the global coordinate system. The upper platform is attached directly to coordinate system Dx'y'z'. Since the shaft is fixed, the upper platform or triangle DEF can only move in the coordinate system Dx'y'z', the angle of DEF w.r.t (with respect to) x' axis is θ, φ is the angle of DEF w.r.t y' axis. In the global coordinate system Axyz, γ is the angle of ABC plane w.r.t the motor's arms placed at G, the angle of ABC plane w.r.t the motor's arms placed at H is δ. The homogeneous transformation matrix of the coordinate system Dx'y'z' is shown as follows:

$$T = \begin{bmatrix} \cos\varphi & \sin\varphi\sin\theta & \sin\varphi\cos\theta & 0 \\ 0 & \cos\theta & -\sin\theta & 0 \\ -\sin\varphi & \cos\varphi\cos\theta & \cos\varphi\cos\theta & 0 \\ 0 & 0 & 0 & 1 \end{bmatrix} \quad (24)$$

From the following equations, the initial position of 3 points D, E and F in the coordinate system Dx'y'z' can be deduced:

$$[D \quad E \quad F] = \begin{bmatrix} 0 & \sqrt{d^2 - e^2/4} & \sqrt{d^2 - e^2/4} \\ 0 & -e/2 & e/2 \\ 0 & 0 & 0 \end{bmatrix} \quad (25)$$

3 points D', E' and F' represent the final state of the mechanism. After finishing rotating around y' axis and x' axis, the position of D', E', and F' are determined as follows:

$$[D' \quad E' \quad F' \quad 1]^T = T \times [D \quad E \quad F \quad 1]^T \quad (26)$$

The position of 3 points D', E', and F' in the global coordinate system Axyz can be deduced:

$$\begin{cases} D' = [0, 0, h] \\ E' = [\sqrt{d^2 - e^2/4}\cos\varphi - e\sin\theta\sin\varphi/2, -e\cos\theta/2, \\ \quad -\sqrt{d^2 - e^2/4}\sin\varphi - e\cos\varphi\sin\theta/2 + h] \\ F' = [\sqrt{d^2 - e^2/4}\cos\varphi + e\sin\theta\sin\varphi/2, e\cos\theta/2, \\ \quad -\sqrt{d^2 - e^2/4}\sin\varphi + e\cos\varphi\sin\theta/2 + h] \end{cases} \quad (27)$$

The coordinates of 3 points A, G and H in the global coordinate system Axyz can be deduced based on the following equations:

$$\begin{cases} A = [0, 0, 0] \\ G = [\sqrt{a^2 - b^2/4} + m\cos\gamma, \ -b/2, \ m\sin\gamma] \\ H = [\sqrt{a^2 - b^2/4} + m\cos\delta, \ a_1/2, \ c\sin\delta] \end{cases} \quad (28)$$

Using the positions of above points and the relationship EG = FH = n, it can be deduced that:

$$\begin{cases} \left\|\overrightarrow{EG}\right\| = e \\ \left\|\overrightarrow{FH}\right\| = e \end{cases} \quad (29)$$

There are 4 variables in equation (29) including α, β, γ and δ. Given the value of γ and δ, by solving the system of 2 linear equations in 2 variables, we can find out the

value of α and β. Similarly, given α and β, the value of γ and δ can also be determined.

In Fig. 7, set a = 45mm, b = 65mm, d = 55mm, h = 120mm, e = 50mm, n = 125mm, m = 25mm. The round dark area shows the workspace of point P, this point is placed fixed above triangle DEF. In the coordinate system Dx'y'z', P = (50, 0, 20) is the initial position of point P. The radius of the round dark is 53.84mm, which forms a sphere with the center placed at point D.

IV. Experiment

With the objective of analyzing the effect of performing expressions, an Open robot was implemented based on the mechanisms designed and analyzed in previous sections. The parameters of facial features for the design were collected through a survey of 50 local people in Vietnam. Experiments were conducted with 100 other people in the locality. This helps to avoid confusion or difficulty recognizing emotions caused by unfamiliar faces. The 3D model of the Open robot is shown in Fig. 8.

Two experiments conducted on the Open robot consist of a motion experiment and a recognition experiment. In the motion experiment, the parameters of the motion capabilities of the Open robot were measured. These parameters were measured manually by 7 experts. Each expert conducted 5 samplings for each parameter. The measurement results with errors greater than 3 times the standard deviation will be eliminated to ensure the confidence level of the results. The value of each parameter is determined by the averaging result of the measurements. The motion experimental results are shown in the Open robot column of Table III including 6 parameters. In addition, Table III contains parameters of Human, robot Romeo, and robot of Ciprian author team.

Figure 8. 3D model of humanoid robot head.

TABLE III. Result of Motion Experiment

Parameter		Human	Open	Romeo	Ciprian
Eye	Pitch	70	72.6	30	80
	Yaw	70	62.7	45	90
Jaw-lip	Pitch	41	49.2	None	None
Neck	Roll	45	42.1	40	70
	Pitch	115	99.6	80	90
	Yaw	140	360	180	110

The results of the motion experiment show that the design method of Open robot has significantly improved the capability to simulate motion. In the research into Romeo robot in 2014, a proposed robot head design method includes eye and neck mechanisms. The neck mechanism of Romeo robot has the capability to simulate motion up to 86.15% compared to the human neck. However, the capability to simulate the eye mechanism is still limited. Later research by Ciprian author team brought outstanding results with capability to completely simulate eye motion. Even the range of eye movements to yaw exceeds the expectation of 20 degrees. Ciprian author team achieved 91.37% capability to simulate human head motion, excluding the Jaw-lip mechanism. The object of this paper is to design mechanisms that completely simulate the motion of the human head. This does not require exceeding the threshold of human head capability. The Open robot is complemented with the jaw-lip mechanism that allows for more movements and expressions. This causes the motion ranges of other mechanisms to be affected. Eye movements to yaw reach 89.57% and roll reach 93.55%. Another improvement is the range of Neck movements to pitch, reaching 86.61%. Overall evaluation, Open robot is capable of simulating up to 94.72% of human head motion including Jaw – lip. The recognition experiment is conducted to evaluate the performance expression of the Open robot. 100 local volunteers with diverse facial features and gender participated in this experiment. Each volunteer received a survey sheet with 7 choices: happy, sad, angry, surprised, disgust, fear, and error. The Open robot performed 6 expressions in random order, which was shown in Fig. 9. Volunteers were asked to choose the expression that best matched each expression the open robot performed. In case they are misunderstood and don't know which expression to choose, they will tick into the error box. The results of recognition experiment are shown in Table IV. The columns and rows in Table IV represent the expression of Open robot and the evaluation results of the volunteers, respectively. Experiment results show that the performance expressions by the open robot are highly appreciated. Expressions are recognized with a minimum rate of 81% (Fear). Happy, sad, and angry expressions were the three expressions with the highest recognition rate.

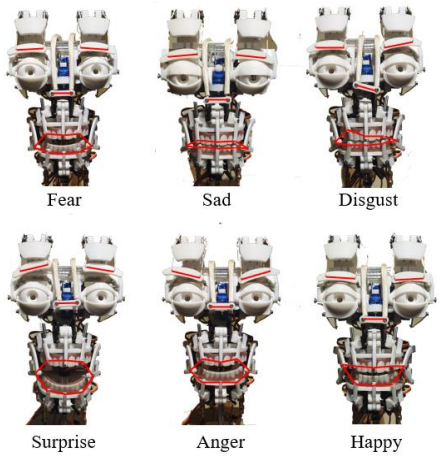

Figure 9. Six expressions of humanoid robot head.

TABLE IV. RESULT OF RECOGNITION EXPERIMENT

%match	Surprise	Happy	Disgust	Sad	Anger	Fear
Surprise	88	0	0	0	4	0
Happy	0	97	0	0	0	0
Disgust	1	1	86	1	0	1
Sad	0	0	0	94	1	4
Anger	3	2	8	0	93	9
Fear	7	0	2	5	2	81
Error	1	0	4	0	0	5

The volunteers did not have any misunderstandings with those expressions (the error column is 0). The reason is that these expressions appear with a high frequency daily. The rest of the expressions had a higher frequency of confusion. Especially, anger expressions are more frequently chosen by volunteers. Out of 115 choose angry expressions, there are 8 confusions that come from disgust and 9 come from fear. In addition, disgust and fear were sometimes misunderstood for the volunteers. This can be explained because Disgust and Fear expressions appear infrequently and all three of these expressions are negative. The overall evaluation of the open robot's expressions has a recognition rate of up to 89.83 %.

V. CONCLUSIONS

This paper presented the mechanical design of the Open robot head including eyes, eyelids, lips, jaw, and neck. FACS was applied to find out appropriate control points and generate Action units, which were combined to create facial expressions. By using anatomical knowledge, we were able to choose a suitable mechanism for each control point and perform kinematics analysis. The results of the experiment shown that the robot head can successfully produce 6 basic facial expressions. By combining with the movement of the neck, there is a variety of expressions can be achieved.

The future work will focus mainly on enhancing the appearance and intelligence of the robot head. A silicone skin will be created and mounted on the robot head so that the it can produce highly realistic facial expressions. Each word the robot head pronouncing will be attached with a different lips shape, this can lead to a big increase in the authenticity of the robot head. The artificial intelligence system will be the core foundation to analyze and recognize the actions and expressions that humans are presenting so that appropriate responses can be given. The system will have the ability to learn and improve recognition through long-term contact with humans.

CONFLICT OF INTEREST

The authors declare no conflict of interest.

AUTHOR CONTRIBUTIONS

Nguyen Khac Toan performed the document preparation, data collection; Le Duc Thuan and Le Bao Long analyzed the results and wrote the first draft of the manuscript; the manuscript was revised by Nguyen Truong Thinh; All authors contributed to conceptualization and design of the study structure and content; all authors had approved the final version.

ACKNOWLEDGMENT

We would like to express our sincere thanks to Ho Chi Minh City University of Technology and Education, Vietnam. This study was supported under the Scientific Research Program of Ho Chi Minh City University of Technology and Education.

REFERENCES

[1] F. Masahiro, "On activating human communications with pet-type robot AIBO," in *Proc. the IEEE*, 2004; vol. 92, pp. 1804-1813,.

[2] Mukai, Hirano, Nakashima, Kato, Sakaida, Guo, et al, "Development of a nursing-care assistant robot RIBA that can lift a human in its arms," in *Proc. 2010 IEEE/RSJ International Conference on Intelligent Robots and Systems*, October 2010, pp. 5996-6001,.

[3] X. X. Ke, Y. J. Zhu, Y. Yang, J. Z. Xin, and Z. T. Luo, et al, "Vision system of facial robot SHFR-III for human-robot interaction," in *Proc. ICINCO*, July 2016, pp. 472-478,.

[4] Pateromichelakis, Mazel, Hache, Koumpogiannis, Gelin, Maisonnier, et al, "Head-eyes system and gaze analysis of the humanoid robot Romeo," in *Proc. 2014 IEEE/RSJ International Conference on Intelligent Robots and Systems*, September 2014, pp. 1374-1379.

[5] C. Lapusan, C. R. Rad, S. Besoiu, Plesa et al, "Design of a humanoid robot head for studying human-robot interaction," in *Proc. 2015 7th International Conference on Electronics, Computers and Artificial Intelligence (ECAI)*, June 2015, pp. WR-15.

[6] Lütkebohle, Hegel, Schulz, Hackel, Wrede, Wachsmuth et al, "The Bielefeld anthropomorphic robot head "Flobi"," in *Proc. 2010 IEEE International Conference on Robotics and Automation*, May 2010, pp. 3384-3391.

[7] M. Zakipour, A. Meghdari, and M. Alemi, "RASA: A low-cost upper-torso social robot acting as a sign language teaching assistant," in *Proc. International Conference on Social Robotics*, pp. 630-639, Springer, Cham, November 2016.

[8] Coşar, Fernandez-Carmona, Agrigoroaie, Pages, Ferland, Zhao, et al, "ENRICHME: Perception and interaction of an assistive robot for the elderly at home," *International Journal of Social Robotics*, vol. 12, pp. 779-805, 2020.

[9] J. Yan, Z. Wang, and Y. Yan, "Humanoid robot head design based on uncanny valley and facs," *Journal of Robotics*, 2014.

[10] Ekman, Paul, and Wallace V. Friesen, "Unmasking the face: A guide to recognizing emotions from facial clues," Vol. 10, Ishk, 2003.

[11] J. Hamm, G. Kohler, R. Verma, , et al, "Automated facial action coding system for dynamic analysis of facial expressions in neuropsychiatric disorders," *Journal of Neuroscience Methods*, vol. 200, pp. 237-256, 2011.

[12] T. Hashimoto, S. Hitramatsu, T. Tsuji, et al, "Development of the face robot SAYA for rich facial expressions," in *Proc. 2006 SICE-ICASE International Joint Conference*, October 2006, pp. 5423-5428.

[13] Neumann, A. Donald, "Kinesiology of the musculoskeletal system-e-book: foundations for rehabilitation," *Elsevier Health Sciences*, 2016.

[14] A. Lefohn, B. Budge, P. Shirley, et al, "An ocularist's approach to human iris synthesis," *IEEE Computer Graphics and Applications*, vol. 23, pp. 70-75, 2003.

[15] S. Alfayad, M. El Asswad, A. Abdellatif, et al, "Hydroïd humanoid robot head with perception and emotion capabilities:

Modeling, design, and experimental results," *Frontiers in Robotics and AI*, 3, 15, 2016.
[16] R. J. Fitzpatrick, "Designing and constructing an animatronic head capable of human motion programmed using face-tracking software," Doctoral dissertation, Worcester Polytechnic Institute, 2012.
[17] S. S. Kenneth, P. Carol, *Anatomy & Physiology: The Unity of Form and Function*, New York, NY, USA: McGraw-Hill, vol. 5 2010.
[18] M. A. Piccinin and P. M. Zito, "Anatomy, head and neck, lips," 2018.
[19] A. J. Andrew and V. C. Quatela, "Quantitative analysis of lip appearance after VY lip augmentation," *Archives of Facial Plastic Surgery*, vol. 6, pp. 172-177, 2004.
[20] Biga, Dawson, Harwell, Hopkins, Kaufmann, LeMaster, et al, *Anatomy &* Physiology, 2020.
[21] T. Muto and M. Kanazawa, "Linear and angular measurements of the mandible during maximal mouth opening," *Journal of Oral and Maxillofacial Surgery*, vol. 54, pp. 970-974, 1996.
[22] F. Dardouri, G. Abba, and W. Seemann, "Parallel robot structure optimizations for a friction stir welding application," in *Proc. ICINCO*, 2017; 2:372-381.

Toan Nguyen Khac was born in Dong Nai Province, Vietnam. He received the B.S. degree in mechatronics engineering from the HCMC University of Technology and Education (HCMUTE) in 2022. His research interests include robots, artificial intelligence, and computer vision. He is responsible for data collection and processing, experiment implementation, and writing the paper.

Thuan Le Duc was born in Dong Nai Province, Vietnam, in 1999. He received the B.S. degree in mechatronics engineering from the HCMC University of Technology and Education (HCMUTE) in 2022. His research interests include power electronics, embedded system applications, and the internet of things. He was responsible for researching and designing the electrical control system for the robot, he took charge of designing the electrical control system and wrote the paper.

Long Bao Le was born in Ba Ria – Vung Tau Province, Vietnam, in 2000. He received the B.S. degree from HCMC University of Technology and Education of Vietnam (HCMUTE). Long Bao Le designed mechanisms such as jaws, lips, eyes, and skull of the robot head and wrote research papers. His research interests include 3D modeling, 3D printing of parts, and technical drawing.